Population of resonance and metastable atoms in a cylindrical volume of finite size

Yuri B. Golubovskii and Alexander Timofeev
Saint-Petersburg State University, Ulyanovskaya 1, St. Petersburg, 198504, Russia

Sergey Gorchakov,* Detlef Loffhagen, and Dirk Uhrlandt
INP Greifswald, Felix-Hausdorff-Straße 2, Greifswald 17489, Germany
(Received 17 October 2008; published 31 March 2009)

A solution method of the Holstein-Biberman equation in the case of two-dimensional finite-size geometry by means of transformation of the integral operator to a four-dimensional matrix is presented. Using this matrix the array of two-dimensional eigenvalues and eigenfunctions of the radiation transport operator in the case of finite cylinder is determined. The exact two-dimensional characteristics have been compared with approximate functions determined as a combination of corresponding eigenvalues and eigenfunctions for the one-dimensional problems (cylinder of infinite length and slab). The spatiotemporal evolution of excited atom densities for two typical forms of the excitation source in a nonequilibrium plasma has been analyzed. The reasons for the distinct difference in the formation of spatiotemporal distributions of resonance and metastable atoms in the case when the spatial distribution of the excitation source does not coincide with the fundamental mode are discussed. Resonance atoms follow the excitation source while the diffusion effectively takes metastable atoms out from the excitation source. Rearrangement of metastable atoms to the fundamental mode during their decay lasts about one effective diffusion lifetime while the corresponding process for the resonance atoms takes much longer (several effective lifetimes). The differences are caused by the effective suppression of higher diffusion modes compared with radiation modes. The developed solution method treats the radiation transport processes at the same accuracy level as diffusion transport of other plasma components and it is suitable for a self-consistent modeling of nonequilibrium plasmas.

DOI: 10.1103/PhysRevE.79.036409 PACS number(s): 52.80.−s, 32.80.−t, 32.50.+d, 02.60.Cb

I. INTRODUCTION

Long-living excited atoms play an important role in gas discharge physics. Metastable and resonance atoms are involved in the processes of stepwise excitation and ionization, chemoionization, and associative ionization, and they participate in the transport of excitation to the working states in gas lasers. The escape of resonance radiation at the tube walls causes the excitation of photoluminescent phosphor and determines the efficiency of luminescent lamps. Long lifetime of atoms affects the properties of afterglow as well as the active phase of pulsed, rf, and microwave discharges [1–4]. The lifetime causes a phase shift between ionization and charged particle density course in alternating fields, and thus, can be a reason for plasma stratification.

The formation of spatiotemporal distributions of metastable and resonance atoms are controlled by different transport mechanisms. The diffusion of metastable atoms is connected with particle transport in the surrounded gas only. In this case, the determination of the corresponding spatiotemporal distribution requires the solution of a partial differential equation with the diffusion operator proportional to the density gradient. Solution methods for such equations are well developed and available even for three-dimensional time-dependent cases. The "diffusion" of the resonance atoms is connected with a number of emission and absorption events since the lifetime of the resonance state is much shorter compared with the characteristic time of the particle movement. At first sight the radiation transport is analogous to the diffusion process, since an excited atom changes its spatial position due to numerous events of re-emission. However, this analogy is rather illusory. The description of a diffusion process is based on the mean-free path of particles. In the case of resonance atoms the photon path between emission and absorption events depends on the frequency the photon was emitted at. If the frequency corresponds to the central part of the spectral line profile, this distance is rather short due to a high value of the absorption coefficient. However, in the case of the profile wings the absorption is weak and the photon can travel a long distance without being absorbed. The calculation of the photon mean-free path in the classical way gives an infinite value, i.e., the photon mean-free path is comparable with the discharge size. Therefore, the description of the transport of excitation due to radiation in the diffusion approach is inadequate, and a more general formulation of the operator which describes the radiation transport is necessary. This operator has an integral form. The balance equation for the density of resonance atoms was formulated in the works of Holstein [5,6] and Biberman [7].

The problem of radiation transport is widely discussed in the literature. A comprehensive review of the radiation transport phenomena in the gas discharge plasma is presented in [8]. The solution of Holstein-Biberman equation is considered in numerous publications (for example [9–27]) for a number of special cases. The spectrum of considered problems spreads from consideration of pure radiation transport, where all other processes are neglected, to complex models which include the Holstein-Biberman equation in the system of fluid equations for different heavy particles [20,25–27].

*gorchakov@inp-greifswald.de

For the description of the discharge plasma the excitation source for each species has to be known. In addition the processes of collisional intermixing between different excited states have to be taken into account. Hence, for the self-consistent description of the discharge a simultaneous solution of the equation system for all plasma components is necessary. In order to achieve the desired accuracy and save computation time, among others a special solution technique for the Holstein-Biberman equation is required. There are numerous analytical and numerical methods for solving the radiation transport equation. Most common is the effective lifetime approach [5,6], which uses the local balancing of the resonance atoms only, while their redistribution in space is not accounted for. This method is accurate enough if the spatial distribution of the excitation rate is close to the fundamental mode. The attempts to include the dependence of effective lifetime on coordinates lead to insignificant improvements only. The most accurate method is the Monte Carlo simulation which can be applied for complex geometry and an arbitrary spectral line profile taking into account possible correlation between absorbed and emitted photon frequencies [17,18]. However, when the total gas pressure exceeds about 100 Pa this method becomes inapplicable in most cases due to computation expenditure.

One of the most promising solution methods for the Holstein-Biberman equation consists in the conversion of the integral radiation transport operator to a matrix which leads to a transformation of the integro-differential equation to a system of linear equations [24]. The effective transition-probability approximation is equivalent to the replacement of the integral radiation transport operator by an expression $A_{\mathrm{eff}}^{\mathrm{res}}I$ where I is the unit matrix and $A_{\mathrm{eff}}^{\mathrm{res}}$ is the effective transition probability for the center of the discharge. In contrast to this, the use of this method [24] leads to the transformation of the integral operator to the matrix $A_{\mathrm{eff}}^{\mathrm{res}}\bar{B}$, where $\bar{B}$ is a full matrix. The diagonal elements of the matrix $\bar{B}$ are equal to 1 and describe the radiative decay of resonance atoms, whereas the nondiagonal elements are negative and correspond to the redistribution of the atoms in space by means of re-emission. This method has been successfully applied for the description of radiation transport in cylindrical geometry with infinite length and for the slab (two infinite parallel plates) in the case of different profiles of spectral line [22,24–26]. However, real plasma sources, such as plasma-chemical reactors or inductively coupled plasma sources (ICP), have plasma sources, have finite size. For this situation the matrix method has to be extended. According to [8] the computation of the matrix elements becomes more complicated because the analytical tricks can no longer be used. For the finite cylinder, we get, e.g., triple integrals. The inversion of the matrix also takes much longer. The authors suggest to use approximate eigenvalues as a sum of eigenvalues of one-dimensional problems and eigenmodes equal to a product of corresponding eigenfunctions of the one-dimensional problems. Using such approximations in [28] the two-dimensional (2D) effects and the saturation in a laser-excited atomic vapor has been studied. The solution of radiative transfer equation for the radiation intensity has been performed using the expansion of the laser intensity into a series of Legendre polynomials and solving the rate equation system for excited states by means of a method similar to the so-called propagator function method [29]. The work [28] includes some simple approximations with error estimates for radiation transport in a finite cylinder. In the case of real multicomponent plasma where the collisional interaction plays an important role and without external radiation source, the system of Holstein-Biberman equations for the densities of resonance atoms has to be solved. Here the matrix methods developed in [24] is the most suitable solution technique. The matrix method avoids any expansions and is free of effective and fitting parameters. It guarantees a high accuracy by low cost of CPU time since the integration over the frequency is made prior to the calculations. As shown in [22,24–26] in the case of one-dimensional geometry, the exact description of radiation transport in the rate equation system for excited states leads to the differences in the absolute densities up to a factor of 2. Consequently, such plasma properties as the ionization balance and output radiation characteristics are strongly influenced by the accuracy of the radiation transport description. For example, the differences in the output power of the low-pressure light sources can reach up to 25% which has been found in better agreement with the experiment [25]. Hence, further development of the matrix method promise not only an accurate description of radiation transport but also more realistic results in numerical models.

In the present work the solution method for the radiation transport equation in a cylinder of finite size is considered. The matrix method suggested in [24] is extended to this condition. For the case of investigations the universal matrix has been determined. The elements of the matrix depend on the ratio of cylinder length to its diameter. The calculated matrix has been used to determine a two-dimensional array of eigenvalues and eigenfunctions. These two-dimensional characteristics are compared with the combination of corresponding characteristics of one-dimensional problems. Using the developed method, the spatiotemporal distributions of the densities of metastable and resonance atoms have been analyzed for the cases with two typical profiles of the excitation source, namely, excitation in the center of the cylinder and on its periphery (skin effect).

II. INITIAL EQUATIONS AND EFFECTIVE TRANSITION-PROBABILITY APPROXIMATION

In the following the radiation transport equation is analyzed for the case when no collisional intermixing between excited states occurs. In this case the balance equation for the density of the resonance atoms including radiation process (Holstein-Biberman equation) reads [5–7]

$$\frac{\partial}{\partial t}N_r(\mathbf{r},t) = W_r(\mathbf{r},t) - G[\mathbf{r},N_r(\mathbf{r},t)]. \tag{1}$$

Here N_r is the density of resonance atoms and W_r is a number of excitation events in the unit volume per second. The radiation transport operator G is determined by

$$G[\mathbf{r},N_r(\mathbf{r},t)] = AN_r(\mathbf{r},t) - A\int_{(V)} N_r(\mathbf{r}',t)K(|\mathbf{r}'-\mathbf{r}|)d\mathbf{r}', \quad (2)$$

where A is the spontaneous transition probability and the kernel $K(|\mathbf{r}'-\mathbf{r}|)$ is the probability for the photons emitted at point $\mathbf{r}'$ to pass the distance $|\mathbf{r}'-\mathbf{r}|$ and to be absorbed at point $\mathbf{r}$. The integration is performed over the whole plasma volume V. The kernel of the integral operator (2) can be represented as [8]

$$K(|\mathbf{r}'-\mathbf{r}|) = \frac{1}{4\pi}\int_0^\infty \varepsilon_\nu k_\nu \frac{e^{-k_\nu|\mathbf{r}'-\mathbf{r}|}}{|\mathbf{r}'-\mathbf{r}|^2}d\nu, \quad (3)$$

where ε_ν and k_ν are emission and absorption line profiles which are assumed to be coincident and normalized according to

$$\int_0^\infty \varepsilon_\nu d\nu = 1, \quad (4)$$

$$k_\nu = k_0\frac{\varepsilon_\nu}{\varepsilon_0}. \quad (5)$$

Here ε_0 and k_0 are the coefficients in the center of the profile.

The radiation transport operator (2) describes the change in the isolated resonance atoms density in time by the spontaneous emission at point $\mathbf{r}$ (first term in the right side) and by the absorption of the photons coming from the whole plasma volume to point $\mathbf{r}$ (second term). Here, the case with a large value of the absorption coefficient (higher than 10) will be considered. This assumption is usually well fulfilled in low- and medium-pressure discharges. The profiles of the absorption and emission lines are supposed to have a Lorentzian form. This is assured if the pressure value exceeds about 1 Pa. These assumptions lead to a simplification of radiation transport operator by a substitution of the asymptotics for the profile wings.

The effective transition-probability approximation by Biberman [7] is based on the assumption that the kernel of the operator $K(|\mathbf{r}'-\mathbf{r}|)$ as a function of distance $|\mathbf{r}'-\mathbf{r}|$ decreases much faster than the atom density N_r does. In this case it is possible to take the value of the density at point $\mathbf{r}$ out of the integral in Eq. (2) and the radiation transport operator gets the representation

$$G[\mathbf{r},N_r(\mathbf{r},t)] = A_{\text{eff}}(\mathbf{r})N_r(\mathbf{r},t), \quad (6)$$

with

$$A_{\text{eff}}(\mathbf{r}) = A\left[1 - \int_{(V)} K(|\mathbf{r}'-\mathbf{r}|)d\mathbf{r}\right] \equiv A\cdot g(\mathbf{r}). \quad (7)$$

Here, $g(\mathbf{r})$ is the escape factor characterizing the decrease of the probability of spontaneous emission due to radiation trapping. It should be mentioned that the effective probability by Biberman [7] differs from the reciprocal effective lifetime by Holstein τ_{eff}^{-1} [5,6] determined as the lifetime of the fundamental mode. In the case of large absorption coefficients the central part of the profile is fully absorbed and the radiation transport occurs due to the wings of the profile.

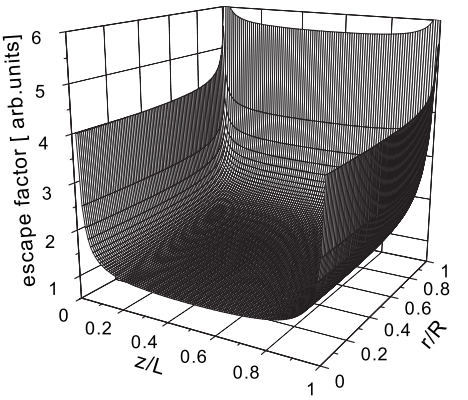

FIG. 1. Dependence of escape factor on the coordinates for finite cylinder.

For a finite-size cylinder the determination of the escape factor requires the fourfold integration over the spatial coordinates and frequency. The derivation of the expression for the escape factor is presented in Appendix A. Figure 1 shows the escape factor in dependence on the radial and axial coordinates for the case when the cylinder length L is equal to its diameter $2R$ and the assumptions given in Appendix A. The increase of the escape probability near the boundary shows that photons emitted near the walls of the cylinder can leave the volume much easier than those released in the center of the cylinder.

III. TRANSFORMATION OF RADIATION TRANSPORT INTEGRAL EQUATION TO A SYSTEM OF LINEAR DIFFERENTIAL EQUATIONS

In case the resonance atom density varies rapidly in scales of the decrease of the kernel $K(|\mathbf{r}'-\mathbf{r}|)$, the approximation of effective transition probability is inadequate and more sophisticated method has to be used. Then, the solution method of Eq. (1) consists in splitting of the whole plasma volume V into the small volumes ΔV_α with integer α. Inside each elementary volume the density of resonance atoms $N_r(\mathbf{r}_\alpha)$ is assumed to be constant. Using the relation $V=\Sigma_\alpha \Delta V_\alpha$ the integral operator [Eq. (2)] gets the representation

$$\int_{(V)} N_r(\mathbf{r}')K(|\mathbf{r}'-\mathbf{r}|)d\mathbf{r} \approx \sum_\alpha N_r(\mathbf{r}_\alpha)\int_{\Delta V_\alpha} K(|\mathbf{r}'-\mathbf{r}|)d\mathbf{r}'. \quad (8)$$

When the radius of the cylinder R and its length L are divided in M_j parts with $\Delta r = R/M_j$ and M_i parts with $\Delta h = L/M_i$, respectively, the elementary volume ΔV_α will be a ring localized in the intervals $r_j < r' < r_{j+1}$, $z_i < z < z_{i+1}$, and $0 < \varphi < 2\pi$. The value of the resonance atom density $N_r(\mathbf{r}_\alpha)$ is replaced by $N_r(r_{j+1/2}, z_{i+1/2})$. Using this discretization the integral Eq. (1) reduces to a system of linear equations

$$\frac{\partial}{\partial t}N_r(r_{m+1/2},z_{n+1/2},t) + \sum_{j=0}^{M_j-1}\sum_{i=0}^{M_i-1} a_{mnji}N_r(r_{j+1/2},z_{i+1/2},t) = W_r(r_{m+1/2},z_{n+1/2},t),$$

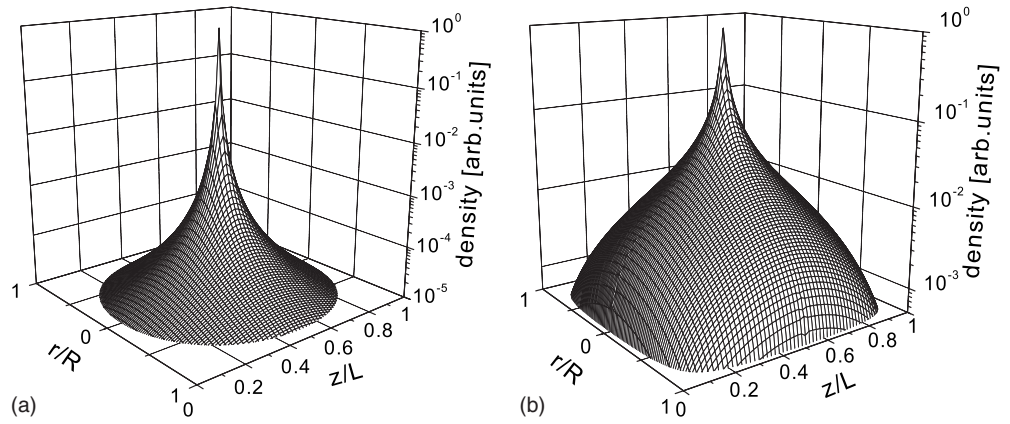

FIG. 2. Spatial distribution of the density of (a) resonance and (b) metastable atoms for a δ-like excitation source.

$$a_{mnji} = A(\delta_{ji}\delta_{mn} - \bar{B}_{mnji}),$$

$$\bar{B}_{mnji} = \int_0^{2\pi} d\varphi \int_{j\Delta r}^{(j+1)\Delta r} r'\,dr' \times \int_{i\Delta z}^{(i+1)\Delta z} K(r_{m+1/2}, z_{n+1/2}, r', z')dz', \tag{9}$$

where δ_{ji} and δ_{mn} are the Kronecker symbols and details of the determination of the matrix coefficients $\bar{B}_{mnji}$ are given in Appendix B. The matrix $\bar{B}$ is universal for a fixed ratio between the length and the diameter of the cylinder at fixed spectral line profile.

After the transformation of the Holstein-Biberman equation [Eq. (1)] by means of the matrix method the densities of the excited atoms as the functions of space and time can be easily found using conventional iterative methods or Gauss method [30]. As an example a stationary spatial distribution of the excited atoms in the cylinder with $L=2R$ for a δ-like excitation source is analyzed. The corresponding excitation source has the form

$$W(r,z) = \begin{cases} 1 & L/2 < z < L/2 + \Delta z, \quad 0 < r < \Delta r \\ 0 & \text{otherwise}, \end{cases} \tag{10}$$

with the parameters $\Delta r = R/30$ and $\Delta z = L/60$. The resulting normalized density profiles are presented in Fig. 2.

The broadening of the spatial distribution of the resonance atom density [Fig. 2(a)] due to the radiation transport processes outward of excitation source is significant near the walls in particular. The normalized density at the wall is about 3 orders of magnitude less than in the center. In the case of the particle diffusion [Fig. 2(b)] the spatial profile is much more broadened. The excitation transport by radiation is, therefore, less effective. The differences in the radiation and diffusion transport mechanisms can be described by means of eigenvalues and eigenfunctions analysis.

IV. EIGENFUNCTION METHOD FOR A FINITE CYLINDER

The eigenfunction method is applicable in the case when no collisional intermixing between the excited levels occurs. First, the case without excitation source is considered. The diffusion equation reads

$$\frac{\partial}{\partial t} N_m(r,z,t) = D_m \left[\frac{1}{r}\frac{\partial}{\partial r}\left(r\frac{\partial}{\partial r} \right) + \frac{\partial^2}{\partial z^2} \right] N_m(r,z,t). \tag{11}$$

Appropriate initial and boundary conditions are

$$N_m\big|_{\substack{r=R \\ z=0,L}} = 0,$$

$$\left.\frac{\partial N_m}{\partial r}\right|_{r=0} = 0,$$

$$N_m|_{t=0} = N_m^0(r,z). \tag{12}$$

Applying the method of separation of variables the solution can be expressed in form of expansion on eigenfunctions according to

$$N_m(r,z,t) = \sum_l \sum_k C_{l,k}^{\text{diff}} e^{-\lambda_{l,k}^{\text{diff}} t} \varphi_{l,k}^{\text{diff}}(r,z). \tag{13}$$

$C_{l,k}^{\text{diff}}$ are the Fourier coefficients of initial distribution expansion, and $\lambda_{l,k}^{\text{diff}}$ and $\varphi_{l,k}^{\text{diff}}(r,z)$ are the two-dimensional eigenvalues and eigenfunctions of the diffusion transport operator. The latter can be expressed as a linear combination of the corresponding characteristics for one-dimensional problems. They read

$$\lambda_{l,k}^{\text{diff}} = D_m \left[\left(\frac{\pi}{L}\right)^2 l^2 + \left(\frac{x_k}{R}\right)^2 \right], \tag{14}$$

$$\varphi_{l,k}^{\text{diff}}(r,z) = \varphi_l^{\text{diff}}(z)\psi_k^{\text{diff}}(r),$$

$$\varphi_l^{\text{diff}}(z) = \sqrt{2}\sin\frac{\pi l z}{L}; \quad \psi_k^{\text{diff}}(r) = \frac{\sqrt{2}}{J_1(x_k)} J_0\left(\frac{r}{R}x_k\right), \tag{15}$$

where x_k is the kth root of zero-order Bessel function, D_m is the diffusion coefficient, and $\varphi_l^{\text{diff}}(z)$ and $\psi_k^{\text{diff}}(r)$ are the one-

TABLE I. 2D array of eigenvalues $\tilde{\lambda}_{l,k}^{\mathrm{res}}$.

l/k	0	1	2	3	4	5	6	7
0	1.269	1.544	1.819	2.077	2.313	2.533	2.737	2.928
1	1.899	2.014	2.169	2.341	2.520	2.698	2.872	3.042
2	2.395	2.459	2.552	2.667	2.796	2.933	3.074	3.216
3	2.812	2.853	2.916	2.997	3.092	3.197	3.309	3.426
4	3.178	3.207	3.252	3.313	3.385	3.467	3.557	3.653
5	3.508	3.529	3.564	3.611	3.668	3.733	3.807	3.887
6	3.810	3.827	3.854	3.892	3.938	3.992	4.053	4.119
7	4.091	4.105	4.127	4.157	4.196	4.241	4.300	4.360

dimensional eigenfunctions for the slab and infinite cylinder, respectively.

In contrast to diffusion problem, the method of separation of variables is inapplicable to the radiation transport operator and the solution of Eq. (1) has to be represented in terms of two-dimensional functions. According to Eq. (14) the radiation transport equation without excitation source results in

$$N_r(r,z,t) = \sum_l \sum_k C_{l,k}^{\mathrm{res}} e^{-\lambda_{l,k}^{\mathrm{res}} t} \varphi_{l,k}^{\mathrm{res}}(r,z). \tag{16}$$

Here, the two-dimensional eigenvalues $\lambda_{l,k}^{\mathrm{res}}$ and eigenfunctions $\varphi_{l,k}^{\mathrm{res}}(r,z)$ cannot be expressed in terms of the corresponding one-dimensional parameters. Thus, the determination of the spatiotemporal density distributions requires the solution of a separate eigenvalue problem. The replacement of the integral radiation transport operator by the matrix according to Eq. (9) reduces this problem to the determination of eigenvalues and eigenvectors of this matrix, i.e.,

$$\sum_{j=0}^{M_j-1} \sum_{i=0}^{M_i-1} a_{mnji} \varphi_{l,k}^{\mathrm{res}}(r_{j+1/2}, z_{i+1/2}) = \lambda_{l,k}^{\mathrm{res}} \varphi_{l,k}^{\mathrm{res}}(r_{m+1/2}, z_{n+1/2}). \tag{17}$$

Table I represents the normalized eigenvalues $\tilde{\lambda}_{l,k}^{\mathrm{res}}$ calculated for the cylinder with $L=2R$. The normalization is performed according to

$$\lambda_{l,k}^{\mathrm{res}} = (A/\pi k_0 R) \tilde{\lambda}_{l,k}^{\mathrm{res}}. \tag{18}$$

The corresponding eigenvalues for one-dimensional problems are given in the Table II.

The ratio $\tilde{\lambda}_{l,k}^{\mathrm{res}}/(\tilde{\lambda}_l^{\mathrm{res}} + \tilde{\mu}_k^{\mathrm{res}})$ between two-dimensional eigenvalues and the sum of the corresponding one-dimensional eigenvalues is presented in Fig. 3(a). The difference reaches about 30% for the high-order modes and grows with increasing mode number.

TABLE II. Eigenvalues for slab $\tilde{\lambda}_l^{\mathrm{res}}$ and infinite cylinder $\tilde{\mu}_k^{\mathrm{res}}$.

l (or k)	0	1	2	3	4	5	6	7
$\tilde{\lambda}_l^{\mathrm{res}}$	0.443	0.732	0.928	1.093	1.234	1.363	1.479	1.588
$\tilde{\mu}_k^{\mathrm{res}}$	0.733	1.212	1.551	1.829	2.072	2.289	2.487	2.672

Figure 3(b) shows the ratio between the exact fundamental mode and the product of fundamental modes of one-dimensional problems $\varphi_{00}^{\mathrm{res}}(r,z)/[\varphi_0^{\mathrm{res}}(r)\cdot\psi_0^{\mathrm{res}}(z)]$. The relative difference reaches about 25% at the periphery. The deviations are even greater for higher modes. Therefore, the spatiotemporal distributions of the excited atom densities differ as well, especially in the case when the excitation source does not coincide with the fundamental mode.

Figure 4 shows the first nine eigenmodes of the radiation transport operator for the cylinder with $L=2R$. With the exception of the fundamental mode (mode 0-0), all the modes show a change in sign. Depending on the spatial distribution of excitation source these modes will contribute to the resulting density profiles of excited atoms. The influence of the high-order modes on the density distribution is demonstrated for a stationary and a decaying plasma in Secs. V and VI, respectively, for typical forms of the excitation source in nonequilibrium plasmas.

V. SPATIAL DISTRIBUTION OF EXCITED ATOM DENSITY IN STATIONARY PLASMA

For the stationary plasma without intermixing between excited states the spatial distributions can be determined using the expansion of the excitation source and excited atom densities on eigenmodes according to

$$W(r,z) = \sum_l \sum_k B_{l,k}^{\mathrm{res,diff}} \varphi_{l,k}^{\mathrm{res,diff}}(r,z), \tag{19}$$

$$N_{r,m}(r,z) = \sum_l \sum_k C_{l,k}^{\mathrm{res,diff}} \varphi_{l,k}^{\mathrm{res,diff}}(r,z), \tag{20}$$

$$B_{l,k}^{\mathrm{res,diff}} = \int_0^R \int_0^L W(r,z) \varphi_{l,k}^{\mathrm{res,diff}}(r,z) r dr dz, \tag{21}$$

$$C_{l,k}^{\mathrm{res,diff}} = \frac{B_{l,k}^{\mathrm{res,diff}}}{\lambda_{l,k}^{\mathrm{res,diff}}}. \tag{22}$$

Following Eq. (23) the expansion coefficients decrease with increasing mode number l,k due to the growth of corresponding eigenvalues. The comparison between the eigenvalues of radiation transport and diffusion operator is shown in Fig. 5. In the case of the radiation transport a larger number of high-order modes contributes to the solution expansion. Furthermore, the eigenvalues of the diffusion operator have higher absolute values and decrease much faster than those of the radiation transport operator with growing mode number. Therefore, the damping factor, which is inversely proportional to the eigenvalues, is higher in the case of diffusion. As a consequence, higher modes are of higher importance for the formation of spatial distribution of resonance atoms than for the metastable atoms.

Figure 6 displays two typical forms of excitation source $W(r,z)$ in nonequilibrium plasmas. Source A corresponds to an excitation which is localized in the center of the volume

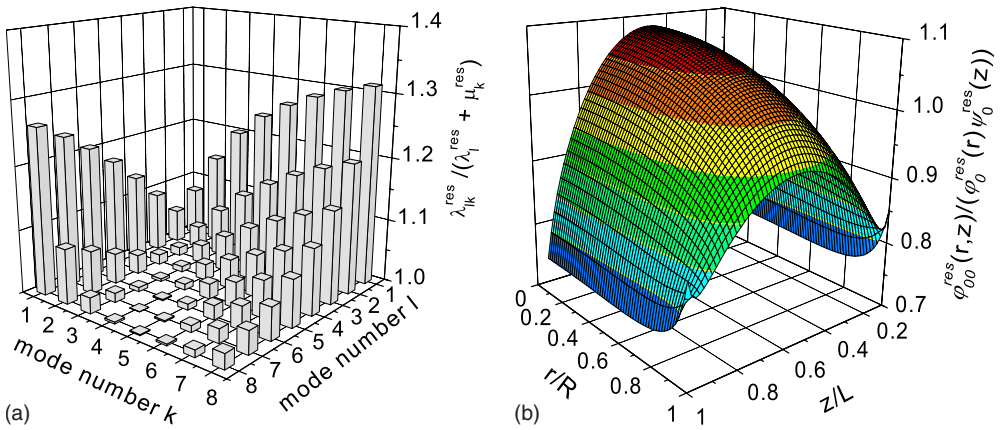

FIG. 3. (Color online) Deviation of (a) approximate eigenvalues from exact eigenvalues of two-dimensional problem and of (b) approximate fundamental mode from the exact one.

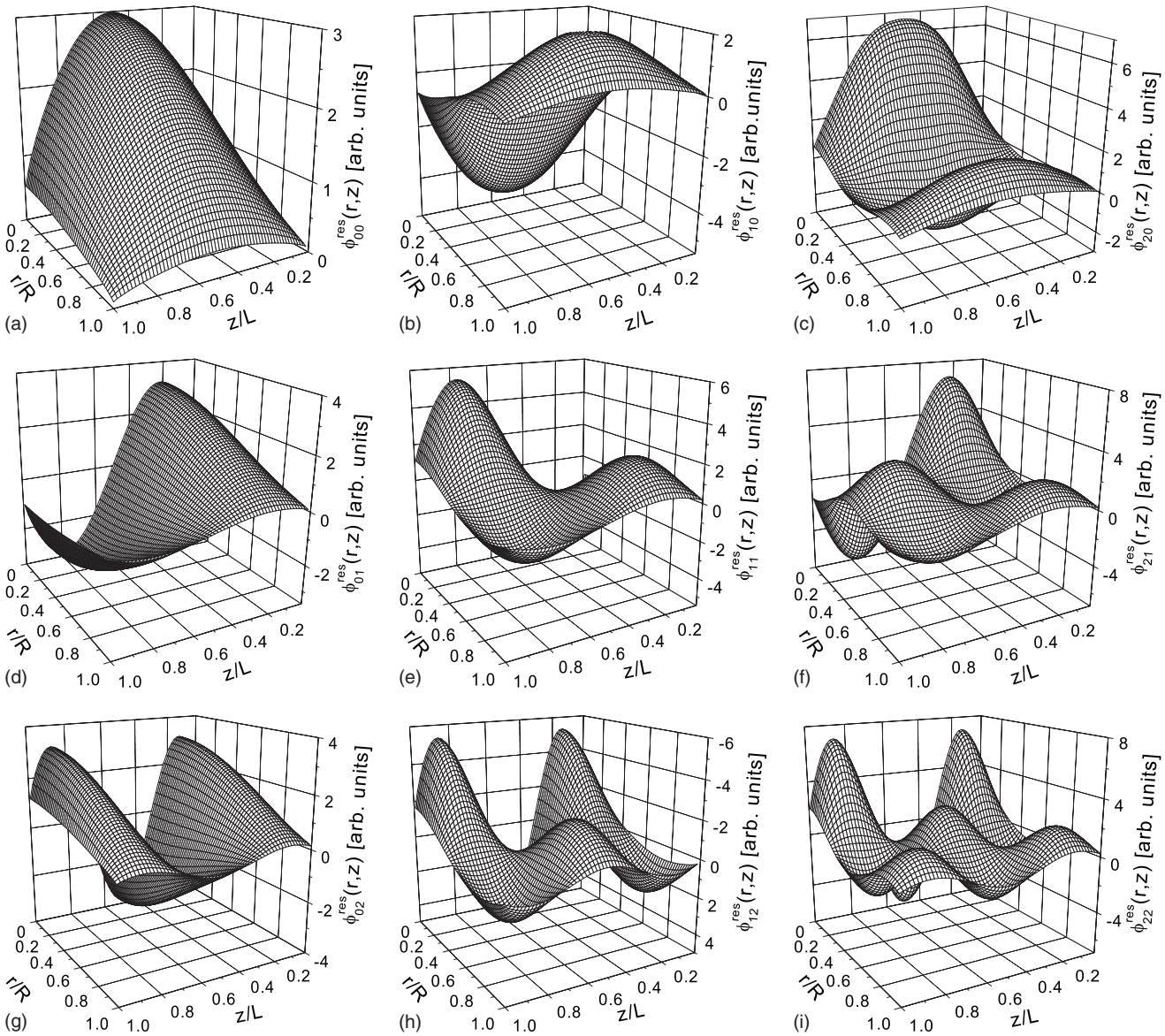

FIG. 4. First nine eigenfunctions of the radiation transport operator.

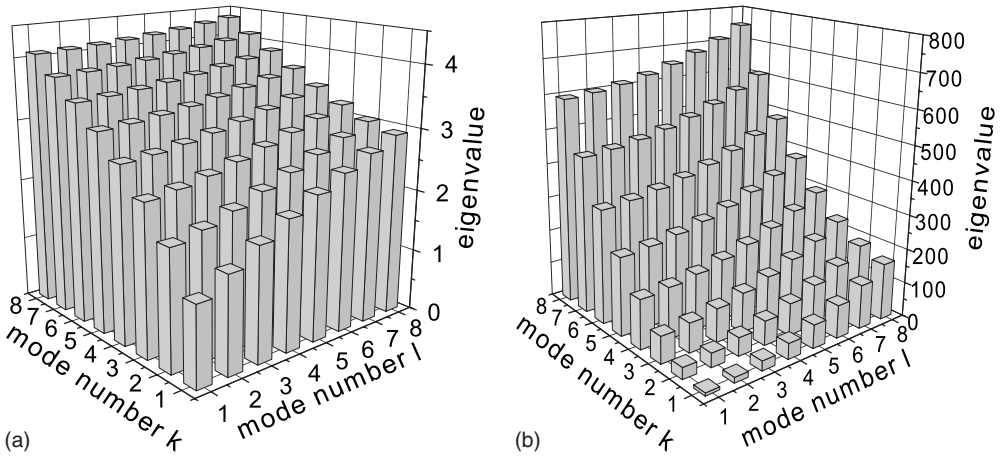

FIG. 5. Two-dimensional array of eigenvalues of (a) radiation transport operator and (b) diffusion operator in the case of a cylinder with $L=2R$.

and source B represents the excitation on the periphery.

A number of modes and a damping factor strongly influence the resulting spatial distributions of corresponding excited atoms. As it is illustrated in Fig. 7, the normalized density of the resonance atoms according to Eq. (20) follows the form of the excitation source, i.e., the transport of excitation outside of the source by radiation is inefficient. In contrast to this, the profiles of the metastable atoms displayed in Fig. 8 are more broadened than those of the corresponding source in Fig. 6. Thus, the damping of the high-order modes leads to an effective excitation transport in space.

VI. DECAY OF EXCITED ATOMS

The differences in diffusion and radiation transport mechanisms correspondingly influence the characteristics of the nonstationary plasma. As an example the decay from an initially given spatial density distribution is considered.

The temporal evolution of resonance and metastable atom densities is described by Eqs. (1) and (11), respectively. Their solutions are given by Eqs. (13) and (16). If the initial density distribution is similar to the fundamental mode, the expansion contains only one term and an exponential decay occurs. The effective lifetime by Holstein for the case of cylinder with $L=2R$ is defined by the expression [5,6]

$$\frac{1}{\tau_{\text{eff}}^{\text{res}}} = \frac{1.269}{\sqrt{\pi k_0 R}} A. \tag{23}$$

The profile of the spatial density distribution in this case is time independent.

When the spectrum of the initial density distribution contains several modes, the decay is characterized by two simultaneous processes: (i) rearrangement of the spectrum to the fundamental mode accompanied by vanishing of high-order modes and (ii) exponential decay of this mode. Due to the more effective suppression of the high-order modes in case of particle diffusion, a different spatiotemporal decay of the metastable and resonance atom densities occurs.

Resulting density distributions for the excitation source localized on the periphery are represented in Figs. 9 and 10 for different instants of the temporal evolution. The density of resonance atoms in Fig. 9 is far from the fundamental mode even after few characteristic decay times $\tau_{\text{eff}}^{\text{res}}$. In the

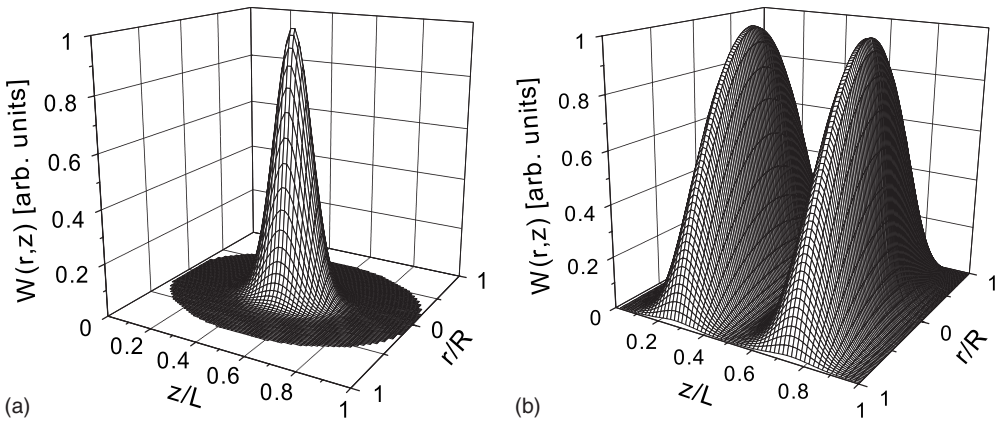

FIG. 6. Typical forms of excitation source in the nonequilibrium plasma; (a) excitation in the volume center (source A) and (b) on its periphery (source B).

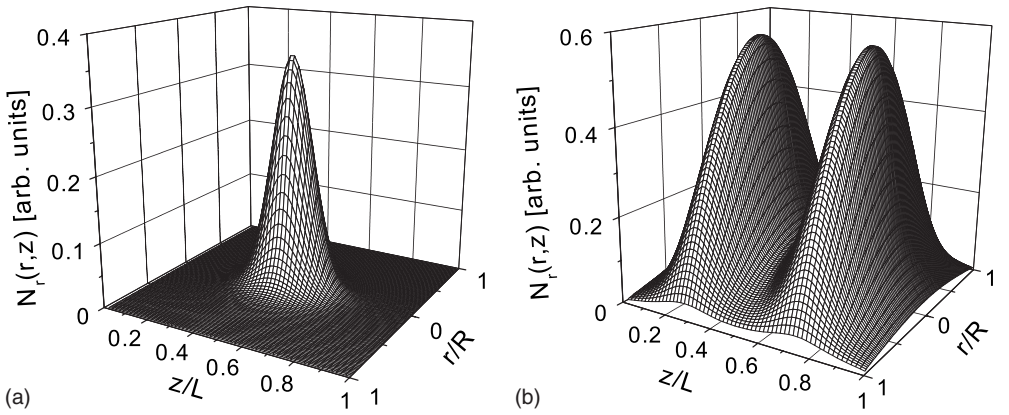

FIG. 7. Spatial distribution of the resonance atoms in the case of (a) excitation source A and (b) excitation source B.

case of particle diffusion (Fig. 10) the distribution follows the fundamental mode after only one characteristic time $\tau_{\text{eff}}^{\text{diff}}$ which is given by

$$\frac{1}{\tau_{\text{eff}}^{\text{diff}}} = D_m\left[\left(\frac{\pi}{L}\right)^2 + \left(\frac{2.405}{R}\right)^2\right]. \tag{24}$$

Analogous results have been obtained for the excitation source localized in the discharge center.

Figures 11 and 12 demonstrate the relaxation of the normalized initial density distribution for resonance and metastable atoms in the case of excitation sources A and B, respectively. The densities are traced for three spatial positions on the cylinder axis, namely, in the center ($r=0$, $z=\frac{1}{2}L$) and in the points with coordinates ($r=0$, $z=\frac{3}{8}L$) and ($r=0$, $z=\frac{1}{4}L$). The decay of the fundamental mode corresponds to a linear dependency of the density on the time in logarithmic scale. The radiation transport requires typically several, i.e., about five to eight effective lifetimes $\tau_{\text{eff}}^{\text{res}}$, for achievement of the distribution corresponding to fundamental mode (Fig. 11). The density of metastable atoms reaches the distribution according to the fundamental mode already after one effective lifetime $\tau_{\text{eff}}^{\text{diff}}$ (Fig. 12). These differences are caused again by suppression of high-order modes of the transport operator.

VII. SUMMARY

The influence of different transport phenomena, i.e., of particle transport and radiation transport, on the spatiotemporal evolution of the densities of excited atoms in a finite-size plasma has been investigated. For the description of the radiation transport the matrix method developed in [24] has been extended and applied. The study has been performed for two typical forms of the excitation source in a nonequilibrium plasma, namely, when the excitation is localized in the volume center and on its periphery.

Using the matrix coefficients the exact two-dimensional eigenvalues and eigenfunctions of the radiation transport operator have been determined. The method of eigenfunctions demonstrates the distinct differences in the transport mechanisms. In the case of radiation transport the two-dimensional eigenvalues and eigenfunctions cannot be expressed as a combination of corresponding parameters of the one-dimensional problems. The deviations which arise from an approximation of the two-dimensional parameters by combination of one-dimensional functions have been evaluated.

The analysis shows that the high-order modes of the transport operator expansion are of great importance for the formation of the spatiotemporal distribution of the densities of excited atoms. Effective suppression of these modes in the case of particle diffusion leads to (i) an effective transport of

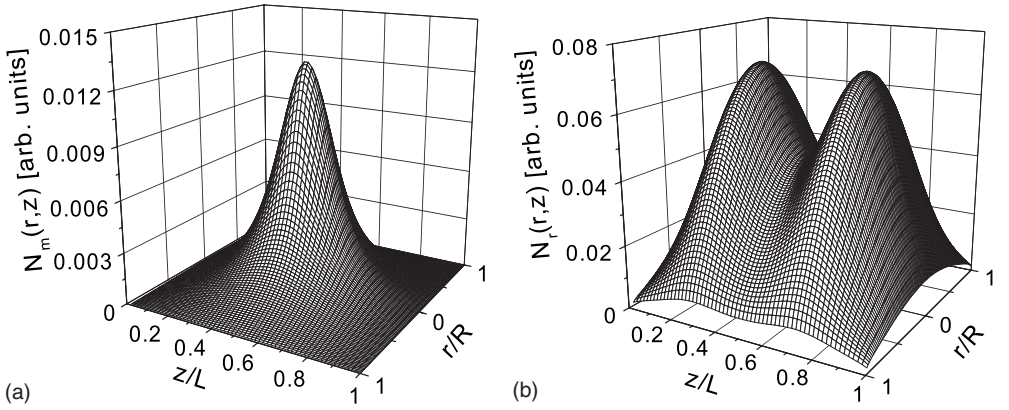

FIG. 8. Spatial distribution of metastable atoms in the case of excitation source localized (a) in the center of the volume and (b) on the periphery.

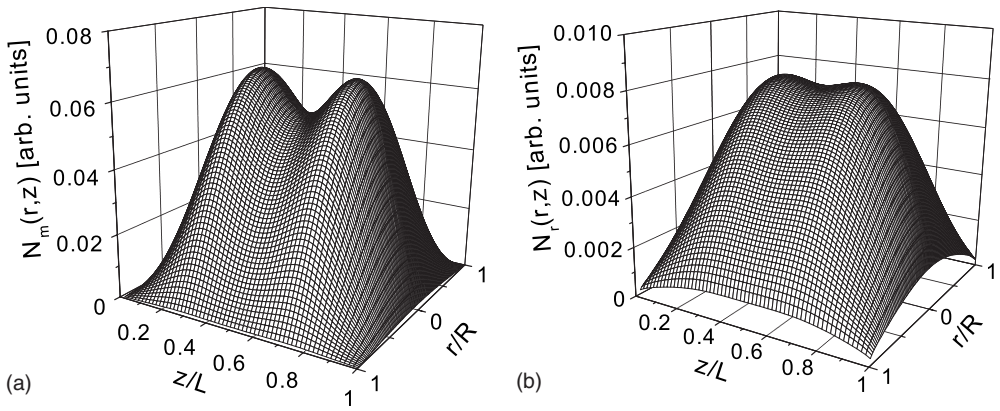

FIG. 9. Spatial distributions of resonance atoms at the instants (a) $2\tau_{\mathrm{eff}}^{\mathrm{res}}$ and (b) $4\tau_{\mathrm{eff}}^{\mathrm{res}}$ in the case of source B.

excitation outside the excitation source and (ii) a fast rearrangement of an arbitrary initial distribution to the fundamental mode in the scale of the effective lifetime. In contrast to this, the radiation transport follows the excitation source in the stationary plasma and it preserves the form of initial distribution for several effective lifetimes in the nonstationary case. The developed solution method treats the radiation transport processes at the same accuracy level as diffusion transport of other plasma components and it is suitable for a self-consistent modeling of nonequilibrium plasmas.

APPENDIX A: DETERMINATION OF THE EFFECTIVE TRANSITION PROBABILITY

In the case of a Lorentz form of the spectral line profile and high absorption coefficients, the central part of spectral line profile is fully absorbed. The radiation transport results from the far wings of the profile and the profile asymptotics can be used. Thus, the emission and absorption coefficients read

$$\varepsilon_\omega = \frac{1}{\pi}\frac{1}{1+\omega^2} \simeq \frac{1}{\pi\omega^2}, \tag{A1}$$

$$k_\omega = \frac{k_0}{1+\omega^2} \simeq \frac{k_0}{\omega^2}, \tag{A2}$$

where $\omega=(\nu-\nu_0)/\Delta\nu$ and $\Delta\nu$ is the half width of Lorentz profile.

To determine the escape factor (7) at point (r,z) it is necessary to include the contributions from all the points (r',z') which follows from the fourfold integration. In the case of finite cylinder of length L and radius R (Fig. 13) the escape factor is given by

$$g(r,z) = 1 - \frac{1}{4\pi}\int_0^{2\pi} d\varphi \int_0^L dz' \int_0^R r'dr' \times \int_{-\infty}^{\infty} \varepsilon_\omega k_\omega \frac{e^{-k_\omega\sqrt{(z-z')^2+q^2(r,r',\varphi)}}}{(z-z')^2+q^2(r,r',\varphi)} d\omega,$$

$$q^2(r,r',\varphi) = r^2 + r'^2 - 2rr'\cos\varphi. \tag{A3}$$

Here φ is the angle between projections of the vectors $\mathbf{r}$ and $\mathbf{r}'$ and q is the distance between the points (r,z) and (r',z'). The angle between the projections of the vectors $\mathbf{q}$ and $\mathbf{r}$ is denoted by ψ. To calculate integral (A3) first the origin of the coordinate system has to be shifted to point (r,z). Then, using the variable transformation $(r',\varphi)\rightarrow(q,\psi)$ and taking into account the equality $r'dr'd\varphi=qdqd\psi$ in Eq. (A3) reads

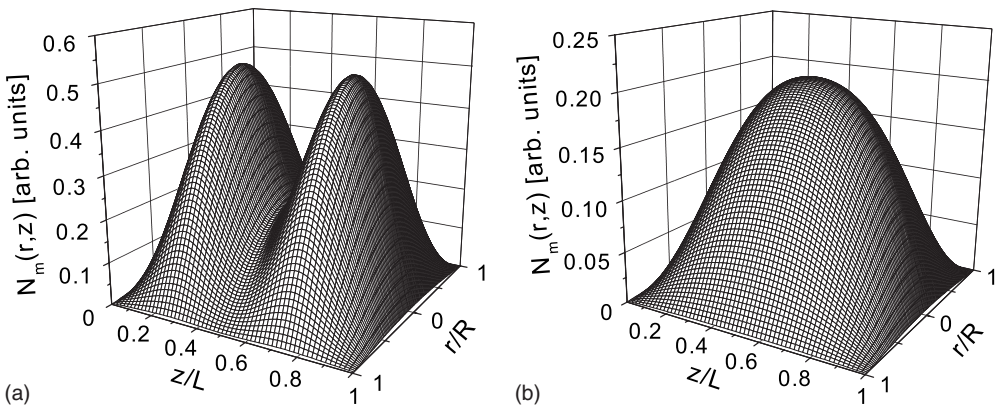

FIG. 10. Spatial distributions of metastable atoms at the instants (a) $0.2\tau_{\mathrm{eff}}^{\mathrm{diff}}$ and (b) $\tau_{\mathrm{eff}}^{\mathrm{diff}}$ in the case of source B.

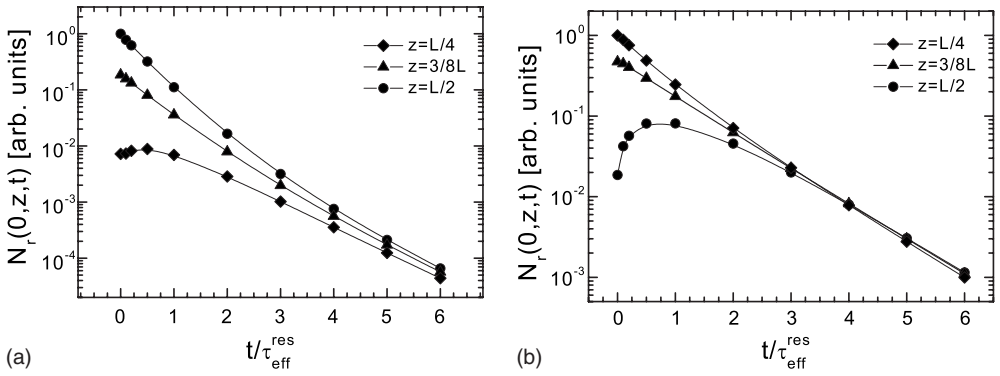

FIG. 11. Transformation to fundamental mode of the density of resonance atoms at three characteristic positions ($r=0$, $z=L/2$; $r=0$, $z=3L/8$; $r=0$, $z=L/4$) in the case of initial distribution concentrated (a) in the center of the cylinder and (b) on its periphery.

$$g(r,z) = 1 - \frac{1}{2\pi}\int_0^{\pi} d\psi \int_{-z}^{L-z} dz' \int_0^{q_0(r,\psi)} qdq \times \int_{-\infty}^{\infty} \varepsilon_\omega k_\omega \frac{e^{-k_\omega q\sqrt{1+(z'/q)^2}}}{q[1+(z'/q)^2]} d\omega, \tag{A4}$$

where

$$q_0(r,\psi) = r\cos\psi + \sqrt{R^2 - r^2\sin^2\psi}$$

is the maximum value of q which is obtained by taking into account the shift of the coordinate system.

It is convenient to introduce the new variable $\xi = z'/q$. Figure 14 shows the area of integration for different geometries. In the case of a cylinder with radius R and length L the determination of the escape factor reduces to the integration over three areas according to

$$g(r,z) = 1 - (I_1 + I_2 + I_3),$$

with

$$I_1 = \frac{1}{2\pi}\int_0^{\pi} d\psi \int_{(L-z)/q_0}^{\infty} d\xi \int_{-\infty}^{\infty} \varepsilon_\omega k_\omega d\omega \int_0^{(L-z)/\xi} \frac{e^{-k_\omega q\sqrt{1+\xi^2}}}{1+\xi^2} dq,$$

$$I_2 = \frac{1}{2\pi}\int_0^{\pi} d\psi \int_{-z/q_0}^{(L-z)/q_0} d\xi \int_{-\infty}^{\infty} \varepsilon_\omega k_\omega d\omega \int_0^{q_0} \frac{e^{-k_\omega q\sqrt{1+\xi^2}}}{1+\xi^2} dq,$$

$$I_3 = \frac{1}{2\pi}\int_0^{\pi} d\psi \int_{z/q_0}^{\infty} d\xi \int_{-\infty}^{\infty} \varepsilon_\omega k_\omega d\omega \int_0^{z/\xi} \frac{e^{-k_\omega q\sqrt{1+\xi^2}}}{1+\xi^2} dq.$$

The integration over coordinate q and frequency ω can be performed analytically. Applying Eqs. (A1) and (A2) the integration yields the relations

$$I_1 = \frac{1}{2\pi}\int_0^{\pi} \left[\int_{(L-z)/q_0}^{\infty} \frac{d\xi}{(1+\xi^2)^{3/2}} - \frac{1}{\sqrt{\pi k_0 (L-z)}} \int_{(L-z)/q_0}^{\infty} \frac{\sqrt{\xi} d\xi}{(1+\xi^2)^{7/4}} \right],$$

$$I_2 = \frac{1}{2\pi}\int_0^{\pi} \left[\int_{-z/q_0}^{(L-z)/q_0} \frac{d\xi}{(1+\xi^2)^{3/2}} - \frac{1}{\sqrt{\pi k_0 q_0}} \int_{-z/q_0}^{(L-z)/q_0} \frac{\sqrt{\xi} d\xi}{(1+\xi^2)^{7/4}} \right],$$

$$I_3 = \frac{1}{2\pi}\int_0^{\pi} \left[\int_{-\infty}^{-z/q_0} \frac{d\xi}{(1+\xi^2)^{3/2}} - \frac{1}{\sqrt{\pi k_0 z}} \int_{-\infty}^{-z/q_0} \frac{\sqrt{-\xi} d\xi}{(1+\xi^2)^{7/4}} \right].$$

After summation the final expression for the escape factor reads

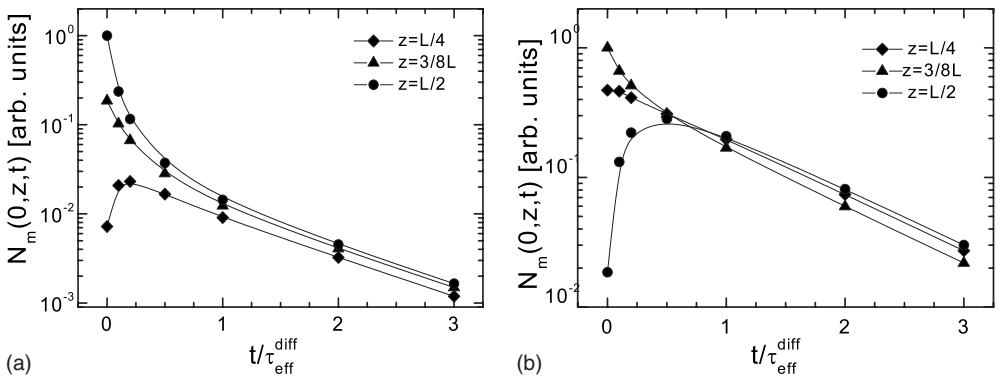

FIG. 12. The same as in Fig. 11 but for the metastable atoms.

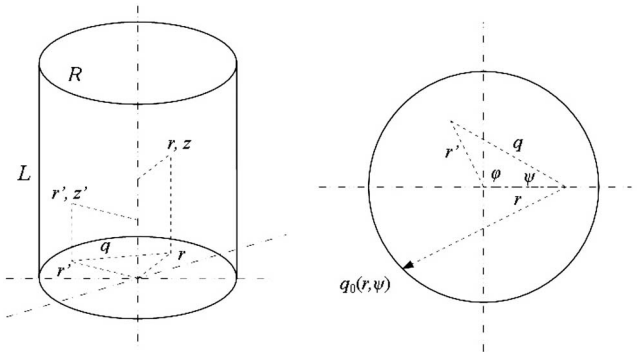

FIG. 13. Limits of integration for finite cylinder (left). Cross section of the cylinder through a plane (right).

$$g(r,z) = \frac{1}{\sqrt{\pi k_0 (L-z)}} \frac{1}{2\pi} \int_0^{\pi} d\psi \int_{(L-z)/q_0(\psi)}^{\infty} \frac{\sqrt{\xi} d\xi}{(1+\xi^2)^{7/4}} + \frac{1}{\sqrt{\pi k_0}} \frac{1}{2\pi} \int_0^{\pi} \frac{d\psi}{\sqrt{q_0(\psi)}} \int_{-z/q_0(\psi)}^{(L-z)/q_0(\psi)} \frac{\sqrt{\xi} d\xi}{(1+\xi^2)^{7/4}} + \frac{1}{\sqrt{\pi k_0 z}} \frac{1}{2\pi} \int_0^{\pi} d\psi \int_{z/q_0(\psi)}^{\infty} \frac{\sqrt{\xi} d\xi}{(1+\xi^2)^{7/4}}. \quad \text{(A5)}$$

APPENDIX B: TRANSFORMATION OF INTEGRAL RADIATION TRANSPORT EQUATION TO A SYSTEM OF LINEAR EQUATIONS

The integral Eq. (1) can be reduced to a system of linear equations in the following way. By means of cylinder discretization the integral term the right-hand side of Eq. (2) without a constant factor A can be replaced by the sum

$$\sum_{i=0}^{N-1} \sum_{n=0}^{M-1} \int_{i\Delta r}^{(i+1)\Delta r} r dr \int_0^{2\pi} d\varphi \int_{n\Delta h}^{(n+1)\Delta h} N_r(r,z) K(r,z,r_j,z_m) dz,$$

$$z_m = (m+1/2)\Delta h, \quad r_j = (j+1/2)\Delta r. \quad \text{(B1)}$$

If the intervals are small enough, the density N_r can be considered to be constant in the respective interval. Thus, it can be extracted according to

$$\sum_{i=0}^{N-1} \sum_{n=0}^{M-1} N_r(r_i,z_n) \int_{i\Delta r}^{(i+1)\Delta r} r dr \int_0^{2\pi} d\varphi \int_{n\Delta h}^{(n+1)\Delta h} K(r,z,r_j,z_m) dz,$$

$$z_n = (n+1/2)\Delta h, \quad r_i = (i+1/2)\Delta r, \quad \text{(B2)}$$

and Eq. (1) gets the representation

$$\frac{\partial N_r(r_j,z_m)}{\partial t} + AN(r_j,z_m) - A \sum_{i=0}^{N-1} \sum_{n=0}^{M-1} N(r_i,z_n) \int_{i\Delta r}^{(i+1)\Delta r} r dr \times \int_0^{2\pi} d\varphi \int_{n\Delta h}^{(n+1)\Delta h} K(r,z,r_j,z_m) dz = W_r(r_j,z_m). \quad \text{(B3)}$$

After rearrangement the final equation for the density of the resonance atoms reads

$$\sum_{i=0}^{N-1} \sum_{n=0}^{M-1} N_r(r_i,z_n)(\delta_{ij}\delta_{nm} - \bar{B}_{injm}) = \frac{1}{A}\left[W_r(r_j,z_m) - \frac{\partial N_r(r_j,z_m)}{\partial t} \right], \quad \text{(B4)}$$

where $\bar{B}$ is the four-dimensional matrix of coefficients

$$\bar{B}_{injm} = \int_{i\Delta r}^{(i+1)\Delta r} r dr \int_0^{2\pi} d\varphi \int_{n\Delta h}^{(n+1)\Delta h} K(r,z,r_j,z_m) dz. \quad \text{(B5)}$$

To determine integral (B5) the matrix of integrals

$$G_{injm} = \int_0^{i\Delta r} r dr \int_0^{2\pi} d\varphi \int_0^{n\Delta h} K(r,z,r_j,z_m) dz \quad \text{(B6)}$$

is used. Then, the elements of the matrix $\bar{B}$ are determined by

$$\bar{B}_{injm} = G_{i+1,n+1,jm} + G_{injm} - G_{i+1,njm} - G_{i,n+1,jm}. \quad \text{(B7)}$$

The form of the integrals in the matrix G depends on the positions (r_i,z_n) and (r_j,z_m) and their relations, respectively. In other words, it depends on indices i, j, m, and n. Four possible combinations of the indices occur: (a) $j \geq i$ and $m \geq n$, (b) $j < i$ and $m < n$, (c) $j < i$ and $m \geq n$, and (d) $j \geq i$ and $m < n$.

(a) $j \geq i$ and $m \geq n$. After the translation of the origin of the cylindrical coordinate system from point (0,0) to point $(r_j,0)$ and the introduction of new differentials $rdrd\varphi dz = qdqd\psi dz$ the matrix elements G_{injm} read

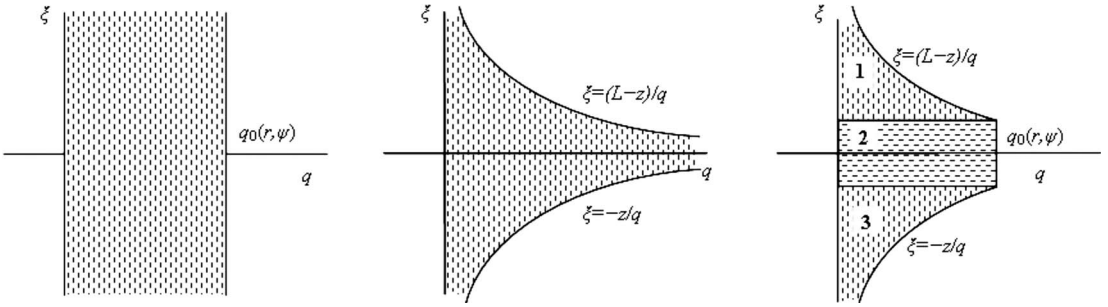

FIG. 14. Integration area (in variables ξ and q); infinite cylinder (left figure), slab (central figure), and finite cylinder (right figure).

$$G_{injm} = 2\int_0^{\psi_m} d\psi \int_0^{z_n} dz \int_{q_-}^{q_+} qdq \int_0^{\infty} \frac{\varepsilon_\nu k_\nu}{4\pi} \frac{e^{-k_\nu\sqrt{q^2+(z_m-z)^2}}}{(z_m-z)^2+q^2} d\nu, \tag{B8}$$

where

$$|\mathbf{r}-\mathbf{r}'| = q^2 + (z_m - z)^2,$$

$$q^2 = r^2 + r_j^2 - 2rr_j\cos\varphi,$$

$$q_+ = r_j\cos\psi + \sqrt{r_i^2 - r_j^2\cos^2\psi},$$

$$q_- = r_j\cos\psi - \sqrt{r_i^2 - r_j^2\cos^2\psi},$$

$$\psi_m = \arcsin\frac{r_{i-1/2}}{r_j}.$$

After the transformation to the variable $\xi=(z_m-z)/q$ the integral expression

$$G_{injm} = 2\int_0^{\psi_m} d\psi \int_{(\xi)} d\xi \int_{q_-}^{q_+} dq \int_{-\infty}^{\infty} \frac{\varepsilon_\omega k_\omega}{4\pi} \frac{e^{-k_\omega q\sqrt{1+\xi^2}}}{1+\xi^2} d\omega \tag{B9}$$

is obtained. The integration over $d\xi dq$ is carried out for the area limited by the curves $\xi=z_m/q$, $\xi=(z_m-z_n)/q$, $q=q_-$, and $q=q_+$. This area has to be divided into three parts with corresponding integration limits. Finally, one gets $G_{injm}=I_1+I_2+I_3$ with

$$I_1 = \frac{1}{2\pi\sqrt{\pi k_0}}\left[\frac{1}{\sqrt{z_m-z_n}}\int_0^{\psi_m} d\psi \int_{(z_m-z_n)/q_+}^{(z_m-z_n)/q_-} \frac{\sqrt{\xi}d\xi}{(1+\xi^2)^{7/4}} - \int_0^{\psi_m} \frac{d\psi}{\sqrt{q_+}} \int_{(z_m-z_n)/q_+}^{(z_m-z_n)/q_-} \frac{d\xi}{(1+\xi^2)^{7/4}}\right],$$

$$I_2 = \frac{1}{2\pi\sqrt{\pi k_0}}\int_0^{\psi_m} d\psi \int_{(z_m-z_n)/q_-}^{(z_m)/q_+} \frac{d\xi}{(1+\xi^2)^{7/4}}\left[\frac{1}{\sqrt{q_-}} - \frac{1}{\sqrt{q_+}}\right],$$

$$I_3 = \frac{1}{2\pi\sqrt{\pi k_0}}\left[\int_0^{\psi_m} \frac{d\psi}{\sqrt{q_-}} \int_{z_m/q_+}^{z_m/q_-} \frac{d\xi}{(1+\xi^2)^{7/4}} - \frac{1}{\sqrt{z_m}}\int_0^{\psi_m} d\psi \int_{z_m/q_+}^{z_m/q_-} \frac{\sqrt{\xi}d\xi}{(1+\xi^2)^{7/4}}\right].$$

Similar operations have to be performed for the other combinations of indices. The final results are given below.

(b) $j<i$ and $m<n$. In this case the integration area is limited by the curves $\xi=z_m/q$, $\xi=(z_m-z_n)/q$, $q=0$, and $q=q_+$. Note that $z_m<z_n$, and the curve $\xi=(z_m-z_n)/q$ lies below the q axis (cf. Fig. 14). Therefore this area again has to be divided into three parts and one obtains

$$G_{injm} = 1 - I_1 - I_2 - I_3,$$

$$I_1 = \frac{1}{2\pi\sqrt{\pi k_0}}\int_0^{\pi} \frac{d\psi}{\sqrt{q_+}} \int_{(z_m-z_n)/q_+}^{(z_m)/q_+} \frac{d\xi}{(1+\xi^2)^{7/4}},$$

$$I_2 = \frac{1}{2\pi\sqrt{\pi k_0}}\frac{1}{\sqrt{z_m}}\int_0^{\pi} d\psi \int_{(z_m)/q_+}^{\infty} \frac{\sqrt{\xi}d\xi}{(1+\xi^2)^{7/4}},$$

$$I_3 = \frac{1}{2\pi\sqrt{\pi k_0}}\frac{1}{\sqrt{z_n-z_m}}\int_0^{\pi} d\psi \int_{-\infty}^{(z_m-z_n)/q_+} \frac{\sqrt{-\xi}d\xi}{(1+\xi^2)^{7/4}}.$$

(c) $j<i$ and $m\geq n$. Now, the integration area is limited by curves $\xi=z_m/q$, $\xi=(z_m-z_n)/q$, $q=0$, and $q=q_+$, and the curve $\xi=(z_m-z_n)/q$ lies above the q axis. Therefore, the matrix element G_{injm} consists of two components, i.e.,

$$G_{injm} = I_1 + I_2,$$

$$I_1 = \frac{1}{2\pi\sqrt{\pi k_0}}\int_0^{\pi} d\psi \int_{(z_m-z_n)/q_+}^{z_m/q_+} \frac{d\xi}{(1+\xi^2)^{7/4}}\left[\frac{\sqrt{\xi}}{\sqrt{z_m-z_n}} - \frac{1}{\sqrt{q_+}}\right],$$

$$I_2 = \frac{1}{2\pi\sqrt{\pi k_0}}\int_0^{\pi} d\psi \int_{z_m/q_+}^{\infty} \frac{\sqrt{\xi}d\xi}{(1+\xi^2)^{7/4}}\left[\frac{1}{\sqrt{z_m-z_n}} - \frac{1}{\sqrt{z_m}}\right].$$

(d) $j\geq i$ and $m<n$. In this case the integration area is limited by the curves $\xi=z_m/q$, $\xi=(z_m-z_n)/q$, $q=q_-$, and $q=q_+$. The matrix element G_{injm} consists of three parts according to

$$G_{injm} = I_1 + I_2 + I_3,$$

$$I_1 = \frac{1}{2\pi\sqrt{\pi k_0}}\int_0^{\psi_m} d\psi \int_{z_m/q_+}^{z_m/q_-} \frac{d\xi}{(1+\xi^2)^{7/4}}\left[\frac{1}{\sqrt{q_-}} - \frac{\sqrt{\xi}}{\sqrt{z_m}}\right],$$

$$I_2 = \frac{1}{2\pi\sqrt{\pi k_0}}\int_0^{\psi_m} d\psi \int_{(z_m-z_n)/q_+}^{z_m/q_+} \frac{d\xi}{(1+\xi^2)^{7/4}}\left[\frac{1}{\sqrt{q_-}} - \frac{1}{\sqrt{q_+}}\right],$$

$$I_3 = \frac{1}{2\pi\sqrt{\pi k_0}}\int_0^{\psi_m} d\psi \int_{(z_m-z_n)/q_-}^{(z_m-z_n)/q_+} \frac{d\xi}{(1+\xi^2)^{7/4}}\left[\frac{1}{\sqrt{q_-}} - \frac{\sqrt{-\xi}}{\sqrt{z_n-z_m}}\right].$$

[1] D. P. Lymberopoulos and D. J. Economou, J. Appl. Phys. **73**, 3668 (1993).

[2] M. W. Kiehlbauch and D. B. Graves, J. Appl. Phys. **91**, 3539 (2002).

[3] T. Sato and T. Makabe, J. Appl. Phys. **98**, 113304 (2005).

[4] S. Gorchakov, D. Loffhagen, and D. Uhrlandt, Phys. Rev. E **74**, 066401 (2006).

[5] T. Holstein, Phys. Rev. **72**, 1212 (1947).

[6] T. Holstein, Phys. Rev. **83**, 1159 (1951).

[7] L. M. Biberman, Zh. Eksp. Teor. Fiz. **17**, 416 (1947).

[8] A. F. Molisch and B. P. Oehry, *Radiation Trapping in Atomic Vapours* (Oxford University Press, Oxford, 1998).

[9] A. F. Molisch, B. P. Oehry, and G. Magerl, J. Quant. Spectrosc. Radiat. Transf. **48**, 377 (1992).
[10] C. van Trigt, Phys. Rev. **181**, 97 (1969).
[11] C. van Trigt, Phys. Rev. A **13**, 734 (1976).
[12] N. N. Bezuglov, A. F. Molisch, A. N. Klucharev, F. Fuso, and M. Allegrini, Phys. Rev. A **57**, 2612 (1998).
[13] N. N. Bezuglov, A. F. Molisch, A. N. Klucharev, F. Fuso, and M. Allegrini, Phys. Rev. A **59**, 4340 (1999).
[14] N. N. Bezuglov and B. V. Taratin, Opt. Spectrosc. **84**, 893 (1998).
[15] A. K. Kazansky, N. N. Bezuglov, A. F. Molisch, F. Fuso, and M. Allegrini, Phys. Rev. A **64**, 022719 (2001).
[16] V. V. Ivanov, *Transfer of Radiation Ion Spectral Lines*, NBS Special Publ. No. 385 (U.S. GPO, Washington, DC, 1973).
[17] J. E. Lawler and J. J. Curry, J. Phys. D **31**, 3235 (1998).
[18] J. E. Lawler, J. J. Curry, and G. G. Lister, J. Phys. D **33**, 252 (2000).
[19] J. P. Apruzese, J. Quant. Spectrosc. Radiat. Transf. **23**, 479 (1980).
[20] J. P. Apruzese, J. Quant. Spectrosc. Radiat. Transf. **25**, 419 (1981).
[21] J. P. Apruzese, J. Quant. Spectrosc. Radiat. Transf. **34**, 447 (1985).
[22] I. A. Porokhova, Yu. B. Golubovskii, C. Csambal, V. Helbig, C. Wilke, and J. F. Behnke, Phys. Rev. E **65**, 046401 (2002).
[23] Yu. B. Golubovskii, I. A. Porokhova, H. Lange, and D. Uhrlandt, Plasma Sources Sci. Technol. **14**, 36 (2005).
[24] Yu. B. Golubovskii, Yu. M. Kagan, and R. I. Lagushchenko, Opt. Spektrosk. **31**, 22 (1971); **38**, 1086 (1975); **40**, 215 (1976).
[25] Yu. B. Golubovskii, I. A. Porokhova, H. Lange, S. Gorchakov, and D. Uhrlandt, Plasma Sources Sci. Technol. **14**, 45 (2005).
[26] Yu. Golubovskii, S. Gorchakov, D. Loffhagen, and D. Uhrlandt, Eur. Phys. J.: Appl. Phys. **37**, 101 (2007).
[27] J. L. Giuliani, G. M. Petrov, J. P. Apruzese, and J. Davis, Plasma Sources Sci. Technol. **14**, 236 (2005).
[28] A. F. Molisch, B. P. Oehry, W. Schupita, and G. Magerl, J. Phys. B **30**, 1879 (1997).
[29] J. E. Lawler, G. Parker, and W. Hitchon, J. Quant. Spectrosc. Radiat. Transf. **49**, 627 (1993).
[30] A. Quarteroni, R. Sacco, and F. Saleri, *Numerical Mathematics* (Springer, Berlin, 2007).